Optical and Quantum Electronics (2024) 56:1439
https://doi.org/10.1007/s11082-024-07381-9

# Design and analysis of a multi-modal refractive index plasmonic biosensor based on split ring resonator for detection of the various cancer cells

**Ali Khodaie**[1] · **Hamid Heidarzadeh**[1]

Received: 26 July 2024 / Accepted: 16 August 2024


**Abstract**
This paper introduces an innovative optical biosensor designed for multimode refractive index (MMRI) detection, employing split ring resonator (SRR) technology for enhanced sensitivity in cancer cell analysis. The proposed biosensor comprises two concentric SRRs, one resembling a cube and the other a cylinder, each incorporating an air gap. Rigorous analysis and optimization of dimensional parameters were conducted using the finite difference time domain (FDTD) numerical solution method. The simulation results demonstrated that the biosensor achieves exceptional sensitivity and an optimal figure of merit (FOM). Specifically, the first mode of the biosensor exhibited a sensitivity exceeding 80 nm/RIU and an FOM surpassing 20 $RIU^{-1}$, while the second mode demonstrated a sensitivity of 570 nm/RIU and an FOM exceeding 4 $RIU^{-1}$. These results indicate that the first mode benefits from a higher FOM, enhancing precision and accuracy, while the second mode benefits from high sensitivity, enabling the detection of minute refractive index changes. With a primary focus on early cancer cell detection and timely treatment initiation to address the global cancer mortality burden, the biosensor's high-quality factor (Q-factor) and FOM promise significant advancements in cancer diagnostics and therapeutic interventions.

**Keywords** Optical biosensor · Plasmonic · Split ring resonator · Cancer cells · Multimode refractive index · Sensitivity

## 1 Introduction

Cancer is one of the leading causes of death globally, according to scientific studies, and researchers have focused their attention on its early detection because it is crucial for initiating an effective treatment regimen (Bray et al. 2018; Yang et al. 2019). There are numerous methods available for the diagnosis of cancer, with tissue biopsy being the prevailing technique utilized globally. In recent years many advances in liquid

✉ Hamid Heidarzadeh
heidarzadeh@uma.ac.ir

[1] Department of Electrical and Computer Engineering, University of Mohaghegh Ardabili, Ardabil, Iran

biopsy technologies have been investigated to detect cancer biomarker (Soda et al. 2022). Nevertheless, in numerous instances, patients who undergo a tissue biopsy may encounter potential risks, including the sampling of tumors situated near vital organs or lesions located in challenging regions of the brain (Robinson et al. 2024). As a result, the exploration for minimally invasive biomarkers plays a critical role in enabling early detection technology with consistent monitoring in tandem with cancer therapy. In recent times, a method called liquid biopsy has been introduced in the medical field to unveil the molecular composition of solid tumors using blood samples. Liquid biopsy has become a widely used medical technique for the identification and surveillance of cancer tumors by detecting various biomarkers such as circulating tumor cells (CTCs), circulating tumor nucleic acids (ctDNA, ctNAs, microRNA), and extracellular vehicles (EVs). Given that these biomarkers can be found in bodily fluids like blood, oral saliva, and urine, liquid biopsy offers a less invasive alternative to tissue biopsy, resulting in reduced pain and lower risk of infection (Wan et al. 2017; Ignatiadis et al. 2021). In recent years, sensor-integrated microfluidic approaches have shown significant promise for liquid biopsy applications in the early detection of cancer, offering enhanced sensitivity and specificity in detecting cancer biomarkers (Sierra et al. 2020). Dielectric grating with a box-like resonance shape as a novel ultra-compact photonic biosensor with a tailored resonance shape has presented in Toma et al. (2024).

The refractive index, electrical permeability, magnetic permeability, and various optical characteristics inherent to biological materials offer valuable insights into their elemental and chemical composition. Consequently, the manipulation of these optical properties in biological samples, coupled with the utilization of optical biosensors, constitutes a critical aspect of optical detection methodologies for analyzing such samples, including cancer cells (Mårtensson Jönsson 2015; Liu et al. 2016). The optical biosensors that have been suggested demonstrate that the identification of extracellular vehicles (EVs) relies on appropriate bio detection components and refractive index (RI) sensitivity. This is due to the fact that the presence of EVs induces a modification in the RI of the specimen. Consequently, it is crucial to establish a photonic sensor architecture that possesses a heightened RI sensitivity in order to achieve real-time, label-free, and effective cancer detection through EV biomarkers (Saha et al. 2022). The design and construction of sensor devices necessitate research and study across diverse disciplines, encompassing engineering sciences, physics, biology, and chemistry. This multidisciplinary approach is essential for the development of sensor technologies that can effectively address complex challenges and meet the demands of diverse applications (Mehrotra 2016; Coulet and Blum 2019). Recent research discussed in Mondal et al. (2024) underscores the significant role of plasmonic biosensors in digital healthcare applications. These biosensors are instrumental in facilitating early disease diagnosis, biomarker monitoring, pathogen detection, and drug screening. By integrating these sensors with digital platforms and smartphone interfaces, real-time data collection, analysis, and transmission are made possible, thereby promoting the transition towards interconnected and readily available healthcare solutions. Jafrasteh et al. introduced a plasmonic sensor designed for the detection of cancer and undertook comprehensive research to assess food contaminants utilizing machine learning and artificial intelligence. Furthermore, they demonstrated that the adverse impacts of environmental pollution on human health can be mitigated through the application of artificial intelligence and machine learning techniques (Jafrasteh et al. 2023). Salehnezhad et al. developed and simulated a highly sensitive plasmonic nanosensor that incorporates monolayer $MoS_2$ and graphene, achieving a sensitivity of 192°/RIU. This innovative sensor is adept at detecting antibodies with refractive indices that closely resemble those of blood groups (Salehnezhad et al. 2023). Furthermore, based on the findings of Farmani et al., a label-free nano sensor utilizing graphene and structured surface plasmon resonance was developed, exhibiting a sensitivity of 333.3 nm/RIU and a figure of merit (FOM) of 16.665 $RIU^{-1}$, aimed at the detection of various biomaterials (Farmani et al. 2020). Hamza et al.'s extensive investigations culminated in the innovation of a three-band microscale biosensor that employs Terahertz MIMs, demonstrating high sensitivity in identifying non-melanoma skin cancer (NMSC) (Hamza et al. 2024). Given the increasing prevalence of life-threatening conditions like cancer, it is imperative for researchers to broaden the application of optical biosensors for the benefit of society. Consequently, further theoretical and experimental investigations are essential for the advancement of optical biosensor design.

In recent years, there has been significant interest and exploration in the study of optical sensors utilizing split ring resonators (SRRs). This burgeoning field has seen the research and development of numerous SRR-based sensors crafted from plasmonic metamaterials, reflecting the growing recognition of their potential in various applications (Jafrasteh et al. 2023; Salehnezhad et al. 2023; Farmani et al. 2020; Hamza et al. 2024; Wellenzohn and Brandl 2015; Abdolrazzaghi et al. 2018; Horestani et al. 2020; Chen et al. 2020; Yang and Lin 2021). Amazing electromagnetic properties, like negative refractive index (Cao et al. 2020), the superlens effect (Chen et al. 2018; Song, et al. 2021) and invisible coating (Jing et al. 2020; Ye et al. 2021), are possessed by metamaterials. The characteristics of metamaterials are frequently interconnected with localized surface plasmon resonances (LSPR), which arise from the collective movements of unbound electrons generating intense electromagnetic fields near the metallic components of the metamaterial (Verma et al. 2024). Pendry et al. (1999) introduced the idea of metamaterial for the first time in 1999. Gold is a plasmonic metamaterial that is crucial to the operation of optical sensors based on SRR as a resonator (Song et al. 2019; Zaitsev et al. 2019). High-sensitivity biosensors are needed today to evaluate various biological samples. This is because there are many deadly diseases in the medical sciences, and diagnosing them calls for sensors with accurate measurement and increased sensitivity (Haq Khan et al. 2023). Throughout the years, a multitude of strategies have been investigated to improve sensitivity in plasmonic applications. These include surface plasmon resonance, optical fibers, optical waveguides, and meta surfaces (Kazanskiy et al. 2022). Because of their high sensitivity and label-free nature, refractive index sensors based on surface plasmon resonance (SPR) and surface plasmon polariton (SPP) currently have many applications in biological processes and medical sciences (Luo et al. 2014; Mandracchia et al. 2015; Wang and Fan 2016; An et al. 2017; Wang et al. 2022; Liu et al. 2023). But because SPR or SPP systems need optical couplers (like prisms and gratings), their production is labor-intensive and expensive due to the need for precise tools (Nootchanat et al. 2019; Benedikovic et al. 2019; Ropp et al. 2023; Laffont, et al. 2023; Flynn et al. 2023). In recent years, researchers have investigated different metal–insulator-metal configurations for plasmonic ring resonators. However, the presence of metal loss in these structures poses a significant challenge as it greatly impacts the quality factor (Wu et al. 2017). Vertical split-ring resonator-based nano plasmonic sensors have demonstrated significant advancements in greatly enhancing sensitivity (Wu et al. 2014). A circuit model for analyzing metal–insulator–metal plasmonic complementary split-ring resonators provides a comprehensive framework for understanding and optimizing their performance in various sensing applications (Bahadori et al. 2014). Optical slot-assisted meta surfaces have shown great potential for IgG protein detection, offering enhanced sensitivity and selectivity in biosensing applications (Brunetti et al. 2024). Here, we present a plasmonic sensor based on a split ring resonator (SRR) to greatly reduce the aforementioned limitations in order to address these issues.

Additionally, SRR structures have multiple reflection resonances, whereas most SPR or SPP structures are single-mode, meaning they cannot cover more than one resonance (Buzavaite-Verteliene et al. 2020; Li, et al. 2021). Applications for structures made with SRR-based metamaterials are numerous and span a wide range of industries. Although SRR structures are easier and less expensive to fabricate than SPR and SPP-based sensors, their sensing area is typically smaller and their FOM is lower. While numerous studies have been carried out to enhance the quality factor of SRR sensors, new types of SRR-based sensors have been presented to improve the sensing area (Ye et al. 2022). In (Ma et al. 2021), a three-stage coupled SRR structure was introduced, and in Mohammadi et al. (2021), an active feedback loop was studied as a means of improving sensor resolution. Nevertheless, these sensors had a comparatively low sensitivity. Applications for structures made with SRR-based metamaterials are numerous and span a wide range of industries. These include active filters, biosensors with high sensitivity for detecting diseases like cancer, and narrowband filters for wireless communication systems. The obtained results demonstrate that the SRR-based sensor has a relatively good sensitivity, FOM, and high-quality factor in the first mode, and high sensitivity and relatively good quality factor in the second mode. These characteristics make the sensor useful for understanding biological processes, diagnosing a variety of diseases, including cancer and in the pharmaceutical industry.

## 2 Structure and method

This section presents the design of the split ring (SRR) resonator-based multi-mode refractive index (MMRI) plasmonic biosensor as well as the simulation approach used to solve the governing equations. This allows for the comparison of performance metrics and the detection of distinct cancer cells in each mode. Figure 1a depicts the three-dimensional cell structure of the suggested sensor unit, which is made up of two split ring resonator (SRR) that are concentric on a quartz substrate, from both the top view (xy plane) as shown in Fig. 1b and the left view (xz plane) as shown in Fig. 1c. As can be seen, the outer SRR (SSR1) has side length d and the inner SRR (SRR2) has the outer radius $r_{max}$ and the inner radius $r_{min}$ and the width $W_r = r_{max} - r_{min}$. SRR2 is positioned within the air cylinder so that SRR1's center has a radius of R. SRR1 is a cube-shaped piece of gold with an air gap of g1 and SRR2 is a cylinder-shaped piece of silver with an air gap of g2. Ha is the definition of the thickness of both SRR1 and SRR2. SRR2 will be separated from SRR1 by a distance of ha, while SRR1 is positioned precisely on the quartz substrate. In the next stages of the work, the value of h and other structural dimensional parameters are scanned for the best possible performance of the suggested sensor. Additionally, the refractive index of the materials that were used-such as gold, silver, and quartz-was taken from the data of Coode Adams (Coode-Adams 1927), Johnson and Christy (Johnson and Christy 1972), and Palik (Handbook of optical constants of solids 1998), respectively. The effect of structural parameters refers to how variations in the geometric characteristics of the sensor device, such as dimensions, shape, or material composition, influence its performance and capabilities. In the context of a split ring resonator (SRR)-based multi-mode refractive index plasmonic biosensor, structural parameters may include the size and shape of the SRRs, the spacing between them, the material properties of the resonator components, and any other relevant geometric features. Table 1 displays the initial values for the structure's dimensional parameters.

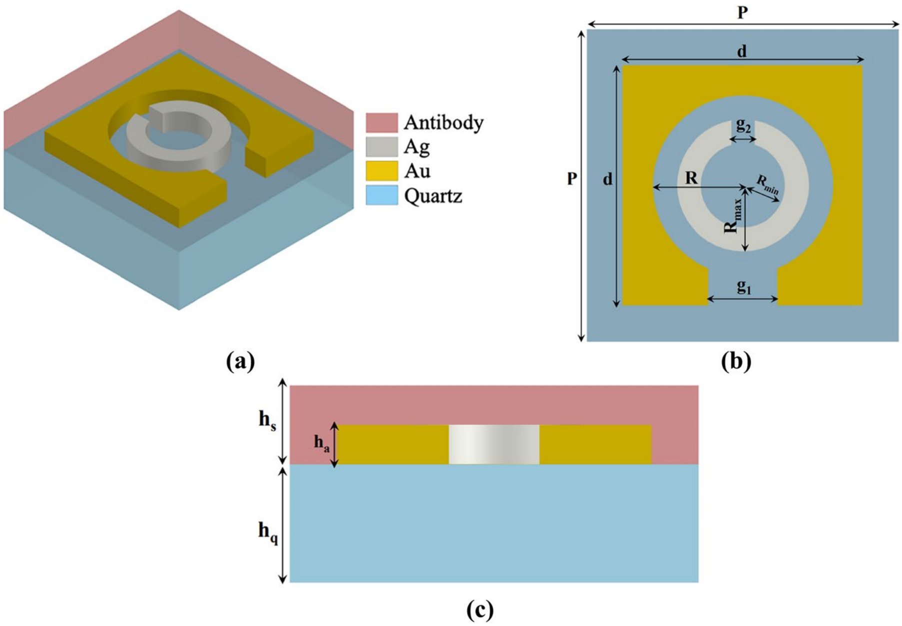


**Fig. 1** **a** 3D schematic of the proposed structure, **b** Top view cross section and **c** Left side view cross section

**Table 1** Dimensional parameters of the proposed structure

| Parameter | Symbol | Value (nm) |
|---|---|---|
| Quartz side length | P | 520 |
| The length of the side of the outer disc | d | 400 |
| The length of the first air gap | g1 | 115 |
| The length of the second air gap | g2 | 38.4 |
| The radius of the air circle inside the disc | R | 150 |
| The outer radius of the ring | rmax | 110 |
| The inner radius of the ring | rmin | 70 |
| Inner ring width (rmax – rmin) | Wr | 40 |
| Quartz height | hq | 150 |
| Disc and ring height | ha | 50 |
| The height of the ring of quartz | h | 0–60 |
| antibody height | hs | 100 |

To compare the performance parameters in each of the modes, the desired structure was simulated using the finite difference time domain (FDTD) numerical solution method. From the top view, a plane wave light source in various wavelengths is projected onto the xy plane with a polarization angle of 0 degrees. Along the x and y axes, periodic boundary conditions are chosen, and Perfectly Matched Layer (PML) boundary conditions are chosen along the z axis. The refractive index of the desired natural

**Table 2** Refractive index values of different cancer cells

| Cells | Cancer cells | RI (n) | References |
|---|---|---|---|
| Normal cell | – | 1.350 | Sharma et al. (2015); Kumar et al. (2017); Jabin et al. (2019); Ahmed et al. (2021) |
| Normal cell<br>Basal | Skin cancer | 1.360<br>1.380 | Sharma et al. (2015); Kumar et al. (2017); Jabin et al. (2019); Ahmed et al. (2021) |
| Normal cell<br>Jurkat | Blood cancer | 1.376<br>1.390 | Sharma et al. (2015); Kumar et al. (2017); Jabin et al. (2019); Ahmed et al. (2021) |
| Normal cell<br>Hela | Cervical cancer | 1.368<br>1.392 | Sharma et al. (2015); Kumar et al. (2017); Jabin et al. (2019); Ahmed et al. (2021) |
| Normal cell<br>PC12 | Adrenal gland cancer | 1.381<br>1.395 | Sharma et al. (2015); Kumar et al. (2017); Jabin et al. (2019); Ahmed et al. (2021) |
| Normal cell<br>MDA-MB-231 | Breast cancer | 1.385<br>1.399 | Sharma et al. (2015); Kumar et al. (2017); Jabin et al. (2019); Ahmed et al. (2021) |
| Normal cell<br>MCF-7 | Breast cancer | 1.387<br>1.401 | Sharma et al. (2015); Kumar et al. (2017); Jabin et al. (2019); Ahmed et al. (2021) |

antibody and different cancer cells are also shown in Table 2. Because the desired structure is created and simulated to detect various cancer cells.

The presence of cancer cells alters the normal antibody's refractive index $(\Delta ns_s)$, and this alteration in refractive index causes a shift in the structure's reflection spectrum's wavelength $(\Delta\lambda_0)$. Consequently, the suggested biosensor's sensitivity (S) is defined as Eq. 1 (Bijalwan et al. 2021).

$$S = \frac{\Delta\lambda_0}{\Delta ns_s} \tag{1}$$

Furthermore, the FOM and quality factor (Q-factor) of the biosensor are expressed as Eq. 2 and Eq. 3, respectively (Yang and Lin 2021; Jalil et al. 2021).

$$FOM = \frac{S}{FWHM} \tag{2}$$

$$Q\text{ - factor} = \frac{\lambda_0}{FWHM} \tag{3}$$

where FWHM is the full width at half maximum.

## 3 Results and discussion

The proposed split ring resonator configurations are investigated to determine the optimal mode concerning material composition and dimensional attributes for the detection of diverse cancer cells. The determination of the most favorable resonant frequencies was conducted through simulations of the biosensor's reflection spectrum across varied wavelengths, as illustrated in Fig. 2, employing gold and silver as materials for SRR1 and SRR2. Examination of the results reveals two distinct scenarios where the most suitable resonances manifest: firstly, when both SRRs are fabricated from silver, and secondly, when SRR1 is composed of gold while SRR2 is made of silver. Figure 2a, e show the reflectance

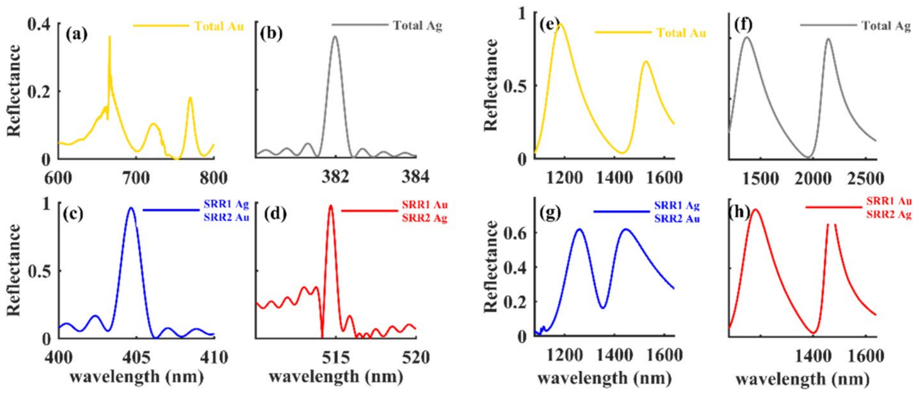


**Fig. 2** **a**, **e** The reflection spectrum of the proposed structure in the first mode (visible wavelength) and the second mode (NIR wavelength) for both Au SRRs, **b**, **f** for both Ag SRRs, **c**, **g** for SRR1 made of Ag and SRR2 made of Au, and **d**, **h** for SRR1 made of Au and SRR2 made of Ag

spectra when both SRRs are made from gold in the visible wavelength and Near-infrared (NIR) wavelength ranges, respectively. Figure 2b, f show the same results when both are made from silver, while Fig. 2c, g illustrate the spectra for SRR1 made of silver and SRR2 made of gold. Finally, Fig. 2d, h present the spectra for SRR1 made of gold and SRR2 made of silver.

The first mode is chosen for the wavelength range of 300–800 nm, while the second mode is selected for the wavelength range of 1000–3000 nm to avoid redundancy. Figure 3a, b depict the contour plot of the reflection spectrum of the proposed structure within the visible and NIR wavelengths, taking into account the distance (h) of SRR2 from the quartz substrate, ranging from 0 to 60 nm. The analysis presented in Fig. 3b reveals that the resonances observed in the second mode exhibit relatively similar characteristics. On the other hand, the resonances in the first mode exhibit significant variations with changes in h, leading to alterations in the resonance wavelength range. The influence of structural parameters on multimodal resonances is a complex interplay involving factors such as geometrical dimensions, material properties, and the electromagnetic environment. Changes in structural parameters like the dimensions of the split ring resonator (SRR), the distance between the SRRs, and the composition of the materials can significantly impact the resonant behavior of the system. For instance, altering the dimensions of the SRRs can lead to shifts in resonant frequencies due to changes in the capacitance and inductance of the structure, affecting the coupling between different modes. Similarly, modifying the distance between SRRs can influence the electromagnetic coupling between them, thereby affecting the mode distribution and resonance frequencies. Furthermore, varying the material composition can change intrinsic properties such as conductivity and permittivity, consequently altering the electromagnetic response of the structure. Understanding the intricate relationships between these parameters is crucial for optimizing multimodal resonances in applications such as biosensors, where precise control over resonance characteristics is essential for sensitive detection.

The sensitivity analysis revealed that changes in SRR dimensions had a significant impact on resonant wavelength. Furthermore, variations in material properties were found to alter the electromagnetic response of the structure, resulting in shifts in resonance frequencies and changes in mode distribution. The following examines how variations in SRR2's width (Wr), antibody thickness ($h_s$), and distance (h) from the quartz substrate

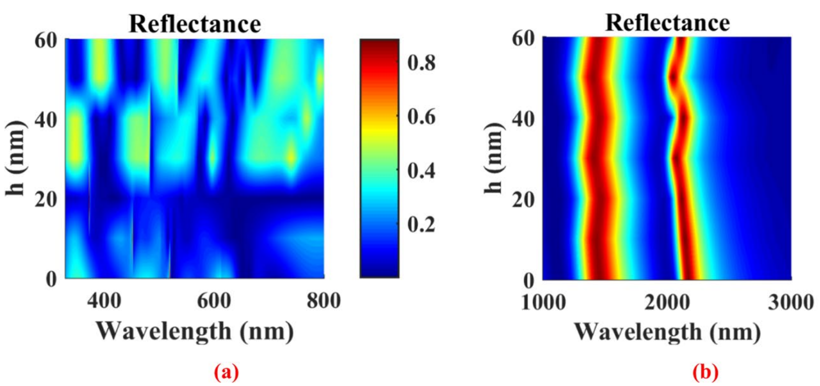


**Fig. 3** **a** contour plot of reflected responses as function of wavelength and h from 0 to 60 nm in the visible wavelength and **b** in the NIR wavelength

affect the sensor's sensitivity and figure of merit for the refractive index of the antibody from 1.33 to 1.41 in one of the resonance modes, from 1000 to 3000 nm. The resonance wavelength diagram in Fig. 4a–c is drawn for Wr = 20–60 nm, h = 0–60 nm, and $h_s$=80 nm–180 nm, respectively. It represents the antibody refractive index from 1.33 to 1.41 in one of the resonance modes, from wavelength 1000 nm to 3000 nm. The sensitivity of the intended sensor is indicated by the graphs' slope. The diagram in Fig. 4a shows that h = 60 nm corresponds to the line with the largest slope based on observations. Additionally, the line with the largest slope in Fig. 4b corresponds to Wr = 20 nm, whereas the line in Fig. 4c does not differ significantly when $h_s$ changes from 80 to 180 nm.

The figure of merit serves as a metric for optimization efforts. Researchers can use it to identify parameters or design features that have the most significant impact on performance and focus their efforts on optimizing those aspects. The sensitivity and FOM diagram for ha changes from 0 to 60 nm are shown in Fig. 5a. As you can see, our preferred wavelength of h = 60 nm had the highest sensitivity and FOM. The impact of variations in SRR2's width (Wr) on the sensor's sensitivity and FOM is examined in the following stage. We only alter $r_{min}$ in this investigation; $r_{max}$ remains constant at 110 nm. Figure 5b from this investigation demonstrates that at Wr = 20 nm, the greatest sensitivity and the smallest FOM occur, and at Wr = 60 nm, the smallest sensitivity and the largest FOM occur. In order to maximize FOM and sensitivity, the best Wr, which is 40 nm, is chosen.

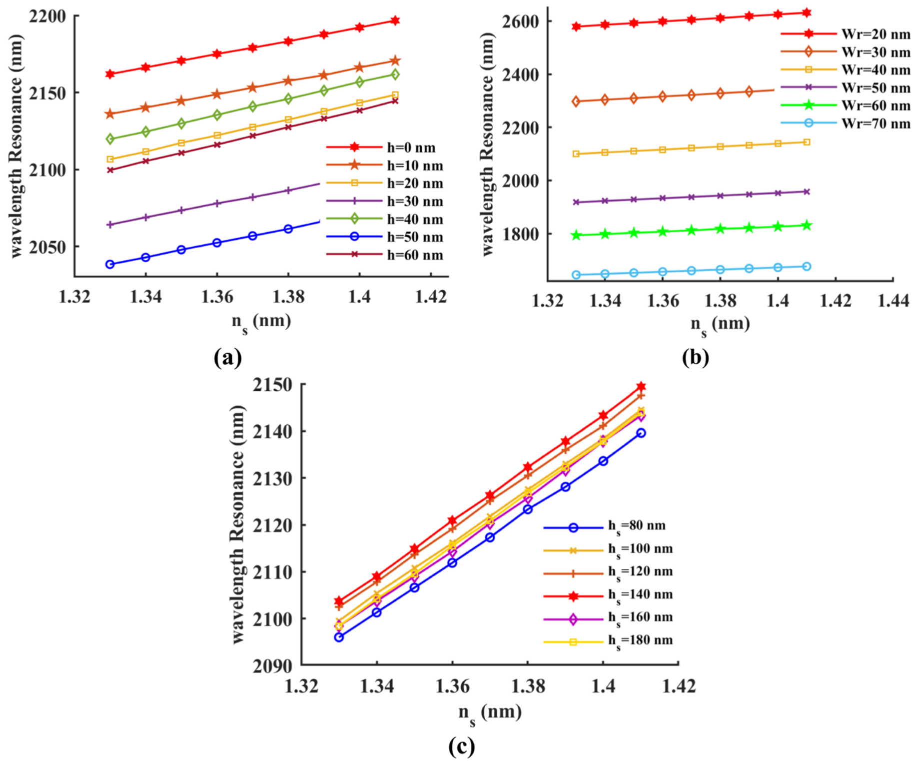


**Fig. 4** **a** Resonance wavelength diagram for antibody refractive index in the second state for h from 0 to 60 nm, **b** for Wr from 20 to 70 nm, and **c** for hs from 80 to 180 nm

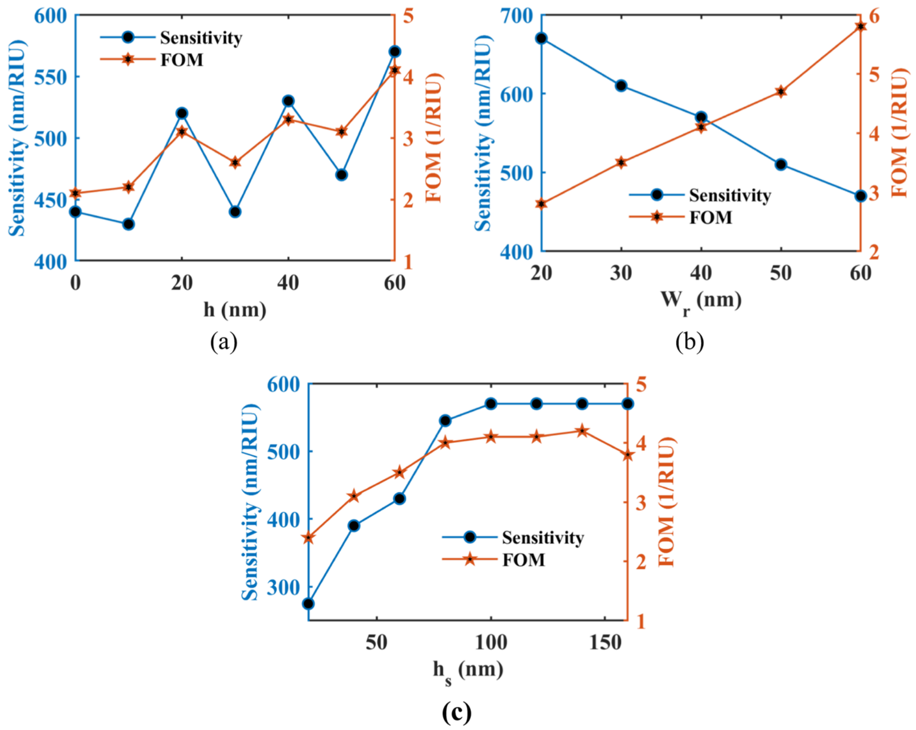


**Fig. 5** **a** sensitivity and FOM in the second mode for h from 0 to 60 nm, **b** per Wr from 20 to 60 nm, and **c** per hs from 20 to 160 nm

This step looks into how the sensitivity and FOM of the sensor are affected by variations in the desired antibody's ($h_s$) thickness. The corresponding diagram, shown in Fig. 5c, shows that, in accordance with the results, the sensor's sensitivity and FOM increase from $h_s$=20 nm to $h_s$=100 nm. However, once $h_s$ exceeds 100 nm, the sensor's sensitivity and FOM virtually remain constant. As a result, we set the antibody's thickness ($h_s$) to 100 nm in this instance. It should be noted that for the investigations conducted in each of these steps, we utilized the second mode described above.

We first evaluate the biosensor in one of the first modes, ranging in wavelength from 300 to 800 nm, in order to identify various cancer cells, after determining the right dimensions for the constructed structure. The reflection spectrum of this state is shown in Fig. 6a. Table 3 displays the outcomes from this section as well. This section yielded the highest sensitivity and FOM, which are 82.5 nm/RIU and 20.53 1/RIU, respectively. These results are superior to those of the biosensor suggested in Ye et al. (2022), which is based on crystal photonics.

Next, the performance parameters are analyzed in second mode, in wavelength ranging from 1000 to 3000 nm. Figure 6b displays the reflection spectrum of the aforementioned state, and Table 4 reports the obtained results. This section shows that the computed FOM and maximum sensitivity are equal to 4.1 1/RIU and 570.4 nm/RIU, respectively. Additionally, it has more optimal results for prostate cancer (PSA) detection than the structure suggested in Shokorlou et al. (2022), which is based on metal–insulator-metal rings.

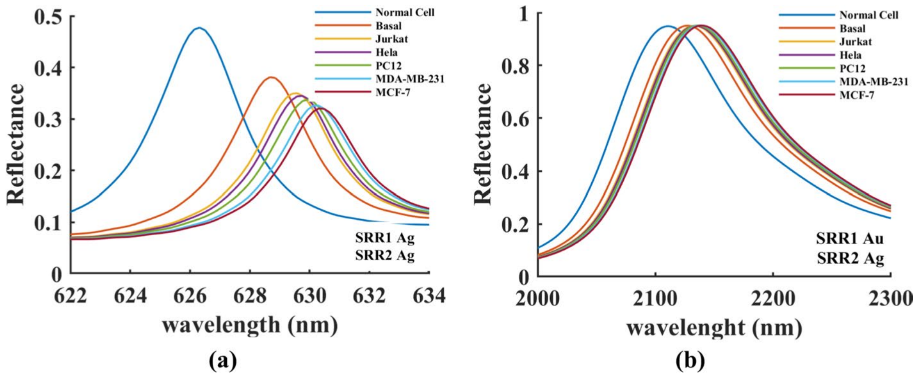


**Fig. 6** **a** The reflection spectrum of the proposed biosensor for the refractive index of cancer cells in the first mode and **b** the second mode

**Table 3** Performance parameters of the proposed biosensor in the first mode

| Cells | Cancer cells | RI (n) | Sensitivity (nm/RIU) | FWHM (nm) | $\lambda_0$ (nm) | Q-factor | FOM |
|---|---|---|---|---|---|---|---|
| Normal cell | – | 1.350 | – | – | 626.30 | – | – |
| Normal cell<br>Basal | Skin cancer | 1.360<br>1.380 | 75.0 | 4 | 627.20<br>628.70 | 157.17 | 18.75 |
| Normal cell<br>Jurkat | Blood cancer | 1.376<br>1.390 | 78.5 | 4.18 | 628.50<br>629.60 | 150.60 | 18.78 |
| Normal cell<br>Hela | Cervical cancer | 1.368<br>1.392 | 82.5 | 4 | 627.78<br>629.76 | 157.44 | 20.53 |
| Normal cell<br>PC12 | Adrenal gland cancer | 1.381<br>1.395 | 75.0 | 4.3 | 628.90<br>629.95 | 146.26 | 17.45 |
| Normal cell<br>MDA-MB-231 | Breast cancer | 1.385<br>1.399 | 79.3 | 4.15 | 629.04<br>630.15 | 151.58 | 19.10 |
| Normal cell<br>MCF-7 | Breast cancer | 1.387<br>1.401 | 77.9 | 4.18 | 629.22<br>630.31 | 150.53 | 18.63 |

Furthermore, compared to values reported in works (Panda et al. 2021; Arafa et al. 2017), the sensitivity of the proposed sensor is significantly higher. When comparing the data from the first and second cases, we find that the sensor's sensitivity in the second case is significantly higher than in the first, but this is not the case for FOM. The resonance wavelength diagram for the cancer cells' refractive index in the two cases under examination is also displayed in Fig. 7. The calculated sensitivity indicator is represented by the slopes of the lines drawn in this diagram; as you can see, the second case's line has a much higher slope than the first case's, which is consistent with the earlier explanation. So, we optimized the design of the plasmonic split ring resonator biosensor by varying key structural parameters such as the ring dimensions, gap size, and material properties. These modifications directly influence the resonant modes of the sensor. Specifically, changes in these parameters affect the electromagnetic field distribution and coupling effects within the resonator, which in turn alter the resonance characteristics. For example, adjusting the gap size can change the strength of the electric field in the split region, thereby shifting the

**Table 4** Performance parameters of the proposed biosensor in the second mode

| Cells | Cancer cells | RI (n) | Sensitivity (nm/RIU) | FWHM (nm) | $\lambda_0$ (nm) | Q-factor | FOM |
|---|---|---|---|---|---|---|---|
| Normal cell | – | 1.350 | – | – | 2110.8 | – | – |
| Normal cell<br>Basal | Skin cancer | 1.360<br>1.380 | 570.40 | 139.22 | 2116.1<br>2127.5 | 15.28 | 4.1 |
| Normal cell<br>Jurkat | Blood cancer | 1.376<br>1.390 | 561.30 | 141.2 | 2125.1<br>2133.0 | 15.1 | 4 |
| Normal cell<br>Hela | Cervical cancer | 1.368<br>1.392 | 553.35 | 140.55 | 2120.9<br>2134.2 | 15.18 | 3.95 |
| Normal cell<br>PC12 | Adrenal gland cancer | 1.381<br>1.395 | 519.50 | 142.30 | 2128.1<br>2135.4 | 15 | 3.65 |
| Normal cell<br>MDA-MB-231 | Breast cancer | 1.385<br>1.399 | 520.70 | 142.50 | 2130.6<br>2137.8 | 15 | 3.66 |
| Normal cell<br>MCF-7 | Breast cancer | 1.387<br>1.401 | 564.50 | 142.80 | 2131.2<br>2139.1 | 14.98 | 3.95 |

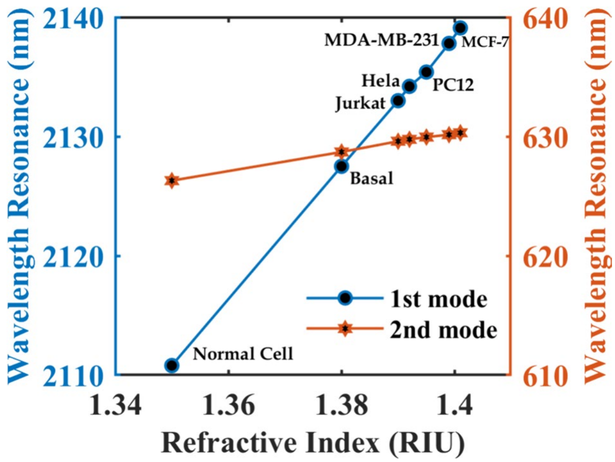


**Fig. 7** Resonance wavelength for refractive index of cancer cells in the first mode and the second mode

resonance frequency and enhancing sensitivity to refractive index changes. Similarly, varying the ring dimensions affects the effective optical path length and can lead to changes in the quality factor and figure of merit. These optimizations are crucial as they directly impact the sensor's performance in terms of sensitivity for different cancer cell types. By systematically studying and fine-tuning these parameters, we have achieved a design that is a multi-modal biosensor.

Two resonances have been found in the reflection spectrum of Fig. 3b, corresponding to the second state. To better understand the electromagnetic responses of the biosensor at these wavelengths, we examine the distribution of the electric and magnetic fields of both SRRs under the assumption that h = 0 nm. The distribution of the electric and magnetic fields at wavelengths of 1367 nm and 2143 nm are depicted in Fig. 8a, b, both in the xy-cross section and from the top view. The magnetic field is primarily dispersed in the area between the two SRRs, while the electric field is primarily distributed inside the gap between SRR1 and SRR2, as well as along the outer walls of SRR1. Additionally, we show

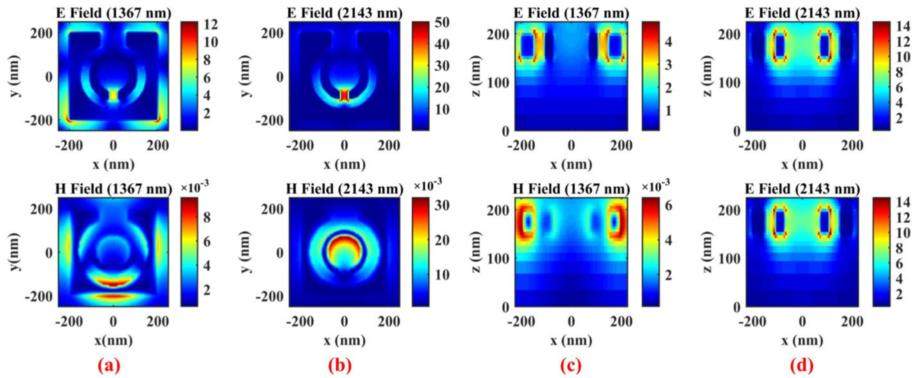


**Fig. 8** **a**, **c** Electric and magnetic field distribution of the sensor for the xy and xz planes, respectively, at the wavelength of 1367 nm. **b**, **d** wavelength 2143 nm

the distribution of the electric and magnetic fields in the xz-cross section and from the left view at wavelengths of 2143 nm and 1367 nm in Fig. 8c, d. To optimize the design of the plasmonic split ring resonator biosensor, we varied key structural parameters such as the ring dimensions, gap size, and material properties. These modifications directly influence the resonant modes of the sensor, which, in this case, are Lorentzian resonant modes.

Figure 9 illustrates the reflection, transmission, and absorption characteristics for both of visible and NIR wavelength ranges. Specifically, Fig. 9a shows the reflection, transmission, and absorption diagram for the wavelength range of 300–800 nm, while Fig. 9b covers the wavelength range of 1000–3000 nm. According these spectra in visible and NIR wavelength ranges, the proposed structure can be used in optical applications, including filters, absorbers and imaging.

The sensor that was designed can be used to detect a variety of diseases, including cancer, as well as environmental processes. It has a high sensitivity in the second mode and a relatively good sensitivity and high FOM. The sensitivity and FOM values can be significantly increased by increasing the number of internal SRRs in the suggested structure (Yang and Lin 2021). Also, Eq. 3, which received less attention in earlier published works,

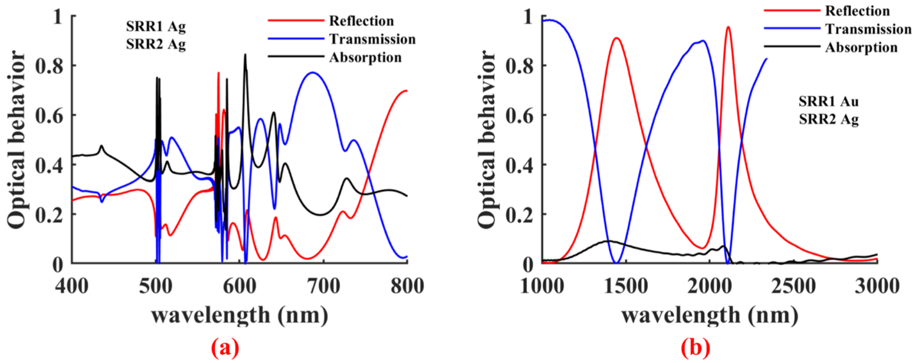


**Fig. 9** **a** Reflection, transmission and absorption diagram for the wavelength range of 400–800 nm, **b** For the wavelength range of 1000–3000 nm

was used in this study to examine the quality coefficient of the designed sensor. Based on the data presented in Tables 3 and 4, the first case's quality factor is significantly higher than the second case's, where the maximum quality factor of 155.44 was achieved. So, our proposed plasmonic SRR biosensor exhibits a higher sensitivity in second mode and higher figure of merit in first mode, which compares favorably with other recently reported sensors. The comparison of sensor performance parameters in both modes with previous works is reported in Table 5. By addressing the current limitations of plasmonic biosensors and leveraging the advantages of SRR design, our proposed sensor provides a balanced solution with improved sensitivity, manufacturability, and practical applicability, making it a strong candidate for early cancer detection and other biomedical applications.

Several approaches exist for the possible development and fabrication of the suggested structure. Nanofabrication methods like electron beam nanolithography (EBL), focused ion beam lithography (FBL), and nanoimprint lithography are among the potential techniques that can be utilized. These techniques offer the opportunity to attain accurate patterning of different materials essential for creating Subwavelength Resonators (SRRs). The sequential assembly of materials necessary for the construction of SRRs can be accomplished by examining various techniques, including layer-by-layer deposition, self-assembly, and transfer printing. These approaches allow for the transfer of prefabricated SRRs from an initial substrate to the final sensor substrate, ensuring smooth integration with various materials. This integration improves the compatibility and performance of the SRRs in the sensor.

## 4 Conclusion

In this study, we developed and simulated a multimode refractive index (MMRI) plasmonic biosensor utilizing a split ring resonator (SRR) architecture for the detection of various cancer cells. Leveraging the Finite-Difference Time-Domain (FDTD) numerical solution method, we analyzed the designed biosensor. First SRR is a cube-shaped piece of Au with an air gap and second SRR is a cylinder-shaped piece of Ag with an air gap. The effect of structural parameters such as dimensions, shape, or material composition, on performance parameters of proposed structure were investigated. Demonstrating promising

**Table 5** Comparison of the performance parameters of the proposed structure with previous works

| References | Base | Sensitivity (nm/RIU) | FWHM (nm) | $\lambda_0$ (nm) | Q-factor | FOM (1/RIU) |
|---|---|---|---|---|---|---|
| Shokorlou et al. (2022) | MIM | 567.23 | 152.35 | 1530 | – | 3.72 |
| Panda et al. (2021) | PC | 290 | – | 621.5 | – | 1074.04 |
| Arafa et al. (2017) | PC | 462 | – | 1600 | $1.11*10^5$ | – |
| Farmani et al. (2020) | SPR | 333.3 | 20 | 1200 | – | 16.665 |
| Bijalwan et al. (2021) | PC | 74.5 | – | 825 | – | 19.6 |
| Shi et al. (2022) | SMRR | 403 | – | 1560 | – | – |
| Goede et al. (2019) | MRR | 100 | – | 1565 | $3.2*10^5$ | – |
| Jian et al. (2017) | MRR | 200 | – | 1560 | $10^4$ | – |
| **This work (1st mode)** | SRR | 82.5 | 4 | 629.76 | 157.44 | 20.53 |
| **This work (2nd mode)** | SRR | 570.4 | 139.22 | 2127.5 | 15.28 | 4.1 |

performance, the biosensor exhibited a sensitivity exceeding 80 nm/RIU and a Figure of Merit (FOM) surpassing 20 $RIU^{-1}$ in the first mode, while in the second mode, it displayed a sensitivity exceeding 570 nm/RIU and an FOM exceeding 4 $RIU^{-1}$. These results highlight the dual benefits of the biosensor: the first mode provides higher precision and accuracy due to its superior FOM, making it ideal for applications requiring detailed and reliable measurements. Meanwhile, the second mode's high sensitivity enables the detection of minute changes in refractive index, which is crucial for early-stage cancer detection and other medical diagnostics. This dual-mode capability enhances the versatility and effectiveness of the biosensor, potentially leading to significant advancements in the field of cancer diagnostics and treatment. The ability to detect and measure small refractive index changes with high sensitivity and precision underscores the biosensor's potential for broad applications in biomedical research and clinical settings.

**Author contributions** All authors contribute equally.

**Funding** The authors have not disclosed any funding.

**Data availability** This manuscript does not report data generation or analysis.

## Declarations

**Conflict of interest** The authors declare no competing interests.

## References

Abdolrazzaghi, M., Daneshmand, M., Iyer, A.K.: Strongly enhanced sensitivity in planar microwave sensors based on metamaterial coupling. IEEE Trans. Microw. Theory Tech.microw. Theory Tech. **66**(4), 1843–1855 (2018)

Ahmed, K., et al.: Numerical demonstration of triangular shaped photonic crystal fibre-based biosensor in the Terahertz range. IET Optoelectron.optoelectron. **15**(1), 1–7 (2021)

An, G., et al.: D-shaped photonic crystal fiber refractive index sensor based on surface plasmon resonance. Appl. Opt. **56**(24), 6988–6992 (2017)

Arafa, S., et al.: Infiltrated photonic crystal cavity as a highly sensitive platform for glucose concentration detection. Opt. Commun.commun. **384**, 93–100 (2017)

Bahadori, M., Eshaghian, A., Mehrany, K.: A circuit model for analysis of metal–insulator–metal plasmonic complementary split-ring resonators. J. Lightwave Technol. **32**(15), 2659–2665 (2014)

Benedikovic, D., et al.: Sub-decibel silicon grating couplers based on L-shaped waveguides and engineered subwavelength metamaterials. Opt. Express **27**(18), 26239–26250 (2019)

Bijalwan, A., Singh, B.K., Rastogi, V.: Analysis of one-dimensional photonic crystal based sensor for detection of blood plasma and cancer cells. Optik **226**, 165994–165999 (2021)

Bray, F., et al.: Global cancer statistics 2018: GLOBOCAN estimates of incidence and mortality worldwide for 36 cancers in 185 countries. CA A Cancer J. Clin. **68**(6), 394–424 (2018)

Brunetti, G., Saha, N., Colapietro P, Ciminelli C.: Optical slot-assisted metasurface for IgG protein detection. In: Journal of physics: conference series 2024 Mar 1, Vol. 2725, No. 1, p 012001. IOP Publishing (2024)

Buzavaite-Verteliene, E., et al.: Hybrid Tamm-surface plasmon polariton mode for highly sensitive detection of protein interactions. Opt. Express **28**(20), 29033–29043 (2020)

Cao, W., Gao, J., Yang, X.: Determination of effective parameters of fishnet metamaterials with vortex based interferometry. Opt. Express **28**(14), 20051–20061 (2020)

Chen, M., et al.: Design of an acoustic superlens using single-phase metamaterials with a star-shaped lattice structure. Sci. Rep. **8**(1), 1861–1869 (2018)

Chen, T., et al.: Design of a terahertz metamaterial sensor based on split ring resonator nested square ring resonator. Mater. Res. Express **7**(9), 095802–095810 (2020)

Coode-Adams, W.: The refractive index of quartz. In: Proceedings of the royal society of London. Series A, containing papers of a mathematical and physical character. **117**(776): 209–213 (1927)
Coulet, P.R., Blum, L.J.: Biosensor principles and applications. CRC Press, Boca Raton (2019)
De Goede, M., et al.: Al 2 O 3 microring resonators for the detection of a cancer biomarker in undiluted urine. Opt. Express **27**(13), 18508–18521 (2019)
Di Toma, A., Brunetti, G., Colapietro, P., Ciminelli, C.: High-resolved near-field sensing by means of dielectric grating with a box-like resonance shape. IEEE Sens. J. (2024). https://doi.org/10.1109/JSEN.2024.3349948
Farmani, H., Farmani, A., Biglari, Z.: A label-free graphene-based nanosensor using surface plasmon resonance for biomaterials detection. Phys. E Low-dimens. Syst. Nanostruct.**116**, 113730–113740 (2020)
Flynn, C., et al.: Fabrication of waveguide directional couplers using 2-photon lithography. Opt. Express **31**(16), 26323–26334 (2023)
Hamza, M.N., Islam, M.T., Koziel, S., Hamad, M.A., Din, I., Farmani, A., Lavadiya, S., Alibakhshikenari, M.: Designing a high-sensitivity microscale triple-band biosensor based on terahertz MTMs to provide a perfect absorber for non-melanoma skin cancer diagnostic. IEEE Photonics J. (2024). https://doi.org/10.1109/JPHOT.2024.3381649
Haq Khan, Z.U., et al.: Brief review: applications of nanocomposite in electrochemical sensor and drugs delivery. Front. Chem. **11**, 1152217 (2023)
Horestani, A.K., Shaterian, Z., Martin, F.: Rotation sensor based on the cross-polarized excitation of split ring resonators (SRRs). IEEE Sens. J. **20**(17), 9706–9714 (2020)
Ignatiadis, M., Sledge, G.W., Jeffrey, S.S.: Liquid biopsy enters the clinic—implementation issues and future challenges. Nat. Rev. Clin. Oncol.clin. Oncol. **18**(5), 297–312 (2021)
Jabin, M.A., et al.: Surface plasmon resonance based titanium coated biosensor for cancer cell detection. IEEE Photonics J. **11**(4), 1–10 (2019)
Jafrasteh, F., Farmani, A., Mohamadi, J.: Meticulous research for design of plasmonics sensors for cancer detection and food contaminants analysis via machine learning and artificial intelligence. Sci. Rep. **13**(1), 15349 (2023)
Jalil, A.T., et al.: High-sensitivity biosensor based on glass resonance PhC cavities for detection of blood component and glucose concentration in human urine. Coatings **11**(12), 1555 (2021)
Jian, A., et al.: Theoretical analysis of microring resonator-based biosensor with high resolution and free of temperature influence. Opt. Eng. **56**(6), 067103–067103 (2017)
Jing, X., et al.: Design of two invisibility cloaks using transmissive and reflective metamaterial-based multilayer frame microstructures. Opt. Express **28**(24), 35528–35539 (2020)
Johnson, P.B., Christy, R.-W.: Optical constants of the noble metals. Phys. Rev. B **6**(12), 4370 (1972)
Kazanskiy, N.L., Khonina, S.N., Butt, M.A.: Recent development in metasurfaces: a focus on sensing applications. Nanomaterials **13**(1), 118 (2022)
Kumar, P., Kumar, V., Roy, J.S.: Dodecagonal photonic crystal fibers with negative dispersion and low confinement loss. Optik **144**, 363–369 (2017)
Laffont, E., et al.: Performance of grating couplers used in the optical switch configuration. Sensors (basel) **23**(22), 90281–902817 (2023)
Li, M.C., et al.: A simple phase-sensitive surface plasmon resonance sensor based on simultaneous polarization measurement strategy. Sensors (basel) **21**(22), 7615 (2021)
Liu, P.Y., et al.: Cell refractive index for cell biology and disease diagnosis: past, present and future. Lab Chip **16**(4), 634–644 (2016)
Liu, H., et al.: Surface plasmonic biosensors: principles, designs and applications. Analyst **148**(24), 6146–6160 (2023)
Luo, Y.H., et al.: Performance of wavelength modulation surface plasmon resonance biosensor. Spectrosc. Spectr. Anal. **34**(5), 1178–1181 (2014)
Ma, J., et al.: Complex permittivity characterization of liquid samples based on a split ring resonator (SRR). Sensors **21**(10), 3385 (2021)
Mandracchia, B., et al.: Surface plasmon resonance imaging by holographic enhanced mapping. Anal. Chem. **87**(8), 4124–4128 (2015)
Mårtensson Jönsson, H.: Biomedical investigation of human muscle tissue using near infrared time-of-flight spectroscopy (2015)
Mehrotra, P.: Biosensors and their applications–a review. J. Oral Biol. Craniofac. Res. **6**(2), 153–159 (2016)
Mohammadi, S., et al.: High-resolution, sensitivity-enhanced active resonator sensor using substrate-embedded channel for characterizing low-concentration liquid mixtures. IEEE Trans. Microw. Theory Tech.microw. Theory Tech. **70**(1), 576–586 (2021)

Mondal, S., Doan, V.H.M., Truong, T.T., Choi, J., Tak, S., Lee, B., Oh, J.: Recent advances in plasmonic biosensors for digital healthcare applications. Biosens. Develop. Chall. Perspect. (2024). https://doi.org/10.1007/s41683-021-00079-0

Nootchanat, S., et al.: Fabrication of miniature surface plasmon resonance sensor chips by using confined sessile drop technique. ACS Appl. Mater. Interfaces **11**(12), 11954–11960 (2019)

Palik, E.D.: Handbook of Optical Constants of Solids, vol. 3. Academic press, Cambridge (1998)

Panda, A., et al.: Graphene-based 1D defective photonic crystal biosensor for real-time detection of cancer cells. Eur. Phys. J. plus **136**(8), 809 (2021)

Pendry, J.B., et al.: Magnetism from conductors and enhanced nonlinear phenomena. IEEE Trans. Microw. Theory Tech.microw. Theory Tech. **47**(11), 2075–2084 (1999)

Robinson, S.D., et al.: A brain metastasis liquid biopsy: where are we now? Neurooncol. Adv. **6**(1), 066 (2024)

Ropp, C., et al.: Scalable and robust beam shaping using apodized fish-bone grating couplers. Opt. Express **31**(24), 40792–40802 (2023)

Saha, N., et al.: Highly sensitive refractive index sensor based on polymer bragg grating: a case study on extracellular vesicles detection. Biosensors **12**(6), 415 (2022)

Salehnezhad, Z., Soroosh, M., Farmani, A.: Design and numerical simulation of a sensitive plasmonic-based nanosensor utilizing MoS2 monolayer and graphene. Diam. Relat. Mater.relat. Mater. **131**, 109594 (2023)

Sharma, P., Sharan, P. and Deshmukh, P.: A photonic crystal sensor for analysis and detection of cancer cells. In: 2015 International conference on pervasive computing (ICPC). IEEE (2015)

Shi, B., et al.: Compact slot microring resonator for sensitive and label-free optical sensing. Sensors **22**(17), 6467 (2022)

Shokorlou, Y.M., Heidarzadeh, H., Bahador, H.: Simulation and analysis of ring shape metal–insulator-metal plasmonic biosensors for the detection of prostate-specific antigen (PSA). Plasmonics **17**(5), 2197–2204 (2022)

Sierra, J., Marrugo-Ramirez, J., Rodriguez-Trujillo, R., Mir, M., Samitier, J.: Sensor-integrated microfluidic approaches for liquid biopsies applications in early detection of cancer. Sensors **20**(5), 1317 (2020)

Soda, N., Clack, K., Shiddiky, M.J.: Recent advances in liquid biopsy technologies for cancer biomarker detection. Sens. Diagn. **1**(3), 343–375 (2022)

Song, Z., et al.: Terahertz toroidal metamaterial with tunable properties. Opt. Express **27**(4), 5792–5797 (2019)

Song, H., et al.: Research progress and development trends of acoustic metamaterials. Molecules **26**(13), 4018 (2021)

Verma, S., Pathak, A.K., Rahman, B.M.A.: Review of biosensors based on plasmonic-enhanced processes in the metallic and meta-material-supported nanostructures. Micromachines (basel) **15**(4), 502 (2024)

Wan, J.C., et al.: Liquid biopsies come of age: towards implementation of circulating tumour DNA. Nat. Rev. Cancer **17**(4), 223–238 (2017)

Wang, D.S., Fan, S.K.: Microfluidic surface plasmon resonance sensors: from principles to point-of-care applications. Sensors (basel) **16**(8), 1175 (2016)

Wang, Q., et al.: Research advances on surface plasmon resonance biosensors. Nanoscale **14**(3), 564–591 (2022)

Wellenzohn, M. and Brandl, M.: A theoretical design of a biosensor device based on split ring resonators for operation in the microwave regime. In Procedia engineering. **120**: pp 865-869 (2015)

Wu, P.C., Sun, G., Chen, W.T., Yang, K.Y., Huang, Y.W., Chen, Y.H., Huang, H.L., Hsu, W.L., Chiang, H.P., Tsai, D.P.: Vertical split-ring resonator based nanoplasmonic sensor. Appl. Phys. Lett. (2014). https://doi.org/10.1063/1.4891234

Wu, C.T., Huang, C.C., Lee, Y.C.: Plasmonic wavelength demultiplexer with a ring resonator using high-order resonant modes. Appl. Opt. **56**(14), 4039–4044 (2017)

Yang, J., Lin, Y.-S.: Design of tunable terahertz metamaterial sensor with single-and dual-resonance characteristic. Nanomaterials **11**(9), 2212 (2021)

Yang, G., et al.: Recent advances in biosensor for detection of lung cancer biomarkers. Biosens. Bioelectron.. Bioelectron. **141**, 111416 (2019)

Ye, K.P., et al.: Invisible gateway by superscattering effect of metamaterials. Phys. Rev. Lett. **126**(22), 227403 (2021)

Ye, W., et al.: An improved split-ring resonator-based sensor for microfluidic applications. Sensors **22**(21), 8534 (2022)

Zaitsev, A., Grebenchukov, A., Khodzitsky, M.: Tunable THz graphene filter based on cross-in-square-shaped resonators metasurface. Photonics. (2019). https://doi.org/10.3390/photonics6040119